Jahn-Teller Effect in the Methane Cation: Rovibronic Structure and the Geometric Phase

H. J. Wörner, R. van der Veen, and F. Merkt

Laboratorium für Physikalische Chemie, ETH Zürich, CH-8093 Zurich, Switzerland

(Received 15 August 2006; published 27 October 2006)

The rovibronic structure in the photoelectron spectrum of CH_4 has been assigned in infrared-vacuum ultraviolet double-resonance experiments and analyzed using an effective tunneling-rotation Hamiltonian. Comparison of theoretical and experimental level structures of CH_4^+ reveals the effect of the geometric phase and establishes that at low energies, the structure and dynamics are governed by a large-amplitude tunneling motion connecting equivalent minima of C_{2v} geometry. The rotationless ground state of CH_4^+ is a tunneling doublet of triply degenerate levels and the lowest level has rovibronic symmetry F_2. The adiabatic ionization energy of CH_4 is 101753.0(15) cm^{-1}.

DOI: 10.1103/PhysRevLett.97.173003 PACS numbers: 31.30.Gs, 31.50.Gh, 32.10.Hq, 33.60.Cv

The Jahn-Teller effect (JTE) is of fundamental importance in understanding the structure and dynamics of molecular systems [1,2]. Whereas the $(E \otimes e)$ JTE, including the role of the geometric phase, is now well understood from the rovibronic structure of a variety of systems, such as H_3 [3], Li_3 [4], Na_3 [5,6], C_5H_5 , and $C_6H_6^+$ [8], to our knowledge, no spectroscopic data have been reported to date at a resolution sufficient to observe the rovibronic level structure and thus to fully characterize the $T \otimes (e + t_2)$ JTE in the T_d, O_h, or I_h point groups [9]. We report here a combined experimental and theoretical investigation of the rovibronic structure of the methane cation in which we could for the first time quantify the structural and dynamical consequences of the $T \otimes (e + t_2)$ JTE, including the role of the geometric phase.

Until the present work the available experimental information on the methane cation was limited to (1) an investigation by electron paramagnetic resonance spectroscopy in a matrix which established the complete exchange of the protons on the experimental time scale in CH_4^+ [10,11], (2) studies by photoelectron spectroscopy which indicated a very strong Jahn-Teller distortion and a stabilization of more than 1 eV [12,13], and (3) rotationally resolved pulsed-field-ionization zero-kinetic-energy (PFI-ZEKE) photoelectron spectra of CH_4^+ and several isotopomers which also indicated extensive tunneling and a C_{2v} equilibrium structure [14–17]. Unfortunately, the rotational structure of the photoelectron spectrum of CH_4, unlike that of CH_2D_2 [15], could not be assigned because of the absence of combination differences.

Theoretical investigations, primarily by *ab initio* methods, have predicted a C_{2v} equilibrium structure for CH_4^+ [18,19], characterized the minimum energy paths connecting the different equivalent minima [19], and calculated the vibronic structure of CH_4^+ [20,21]. In addition, one-dimensional tunneling calculations have been reported that explained the vibrational structure of CH_4^+ and its deuterated isotopomers at low energies but were not adequate to describe the rotational structure of CH_4^+ nor to assess the role of the geometric phase [16].

On the basis of previous studies, one expects that the 12 equivalent C_{2v} equilibrium structures form two enantiomeric sets of six structures each and that the barriers between the minima within a given set are much lower than the barriers connecting the minima of the two sets (see Fig. 1)[19]. At low energies and an experimental resolution of 0.3 cm^{-1}, the only feasible permutations of the protons are those interconverting the structures within one set; consequently, only six C_{2v} structures need be considered in the treatment of the large-amplitude motion, and the problem can be treated in the $T_d(M)$ group. If the inversion motion

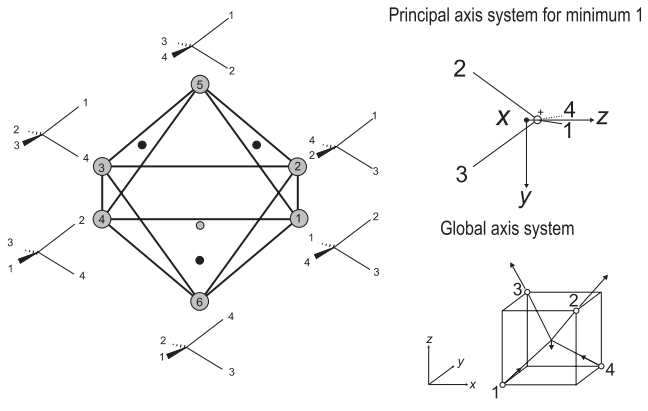

FIG. 1. Left-hand side: set of six equivalent C_{2v} structures of CH_4^+. The vertices correspond to the C_{2v} minimum energy geometries and the edges to equivalent tunneling paths connecting the minima via C_s transition states. Four faces of the octahedron correspond to a C_{3v} geometry with a degenerate ground state (marked with a dot) and the other four to a C_{3v} geometry with a nondegenerate ground state [17]. Right-hand side: Principal axis system chosen for minimum 1 (upper half) and the global axis system defined with respect to the undistorted geometry (lower half). The arrows indicate the distortion that leads from the tetrahedral geometry to distorted C_{2v} structure 1.

leading to the structures of the enantiomeric set becomes feasible, the appropriate group is S_4^*. The correlation of the representations of $T_d(M)$ to S_4^* with spin-statistical weights in parentheses is then $A_1(5) \rightarrow A_1^+(0) \oplus A_2^-(5)$, $A_2(5) \rightarrow A_2^+(5) \oplus A_1^-(0)$, $E(2) \rightarrow E^+(1) \oplus E^-(1)$, $F_1(3) \rightarrow F_1^+(3) \oplus F_2^-(0)$, and $F_2(3) \rightarrow F_2^+(0) \oplus F_1^-(3)$. An inversion splitting will thus only be observable in levels of rovibronic E symmetry. The Jahn-Teller active modes in CH_4^+ are the e bending mode (ν_2) and the two f_2 modes (ν_3 asymmetric stretch and ν_4 bending).

In the experimental part of this work, the nuclear spin symmetry of the rovibronic levels of CH_4^+ was determined in double-resonance experiments. The nuclear spin symmetries with nonzero spin-statistical weight are A_1, E, and F_2 and correspond to the rovibronic symmetries $A_{1,2}$, E, and $F_{1,2}$ respectively. In the theoretical part, an effective tunneling-rotation Hamiltonian was developed in combination with a global axis system analogous to that used to treat local modes in polyatomic molecules [22].

Methane in a pulsed supersonic expansion was photoexcited to the region of the first adiabatic ionization threshold using IR-VUV double-resonance schemes involving selected rotational levels of the $\nu_3 = 1$ vibrational state. The positions of the ionization thresholds corresponding to the different rovibronic energy levels of CH_4^+ were determined by PFI-ZEKE photoelectron spectroscopy [23]. IR radiation at 3.3 μm was generated by difference-frequency mixing in a $KTiOAsO_4$ (KTA) crystal [24]. The pulse energies ($\approx$200 μJ) and diameter ($\approx$2 mm) of the IR beam sufficed to saturate the IR transitions. VUV radiation between 97000 and 102000 cm^{-1} was generated by resonance-enhanced four-wave mixing in xenon as described in [14]. The counterpropagating IR and VUV laser beams crossed the molecular beam at right angles, and the IR pulse preceeded the VUV pulse by $\approx$ 10 ns. Only the lowest level of each nuclear spin symmetry species (A_1, $J = 0$; F_2, $J = 1$; E, $J = 2$) was significantly populated at the low temperature of the supersonic expansion ($T_{rot} < 10$ K).

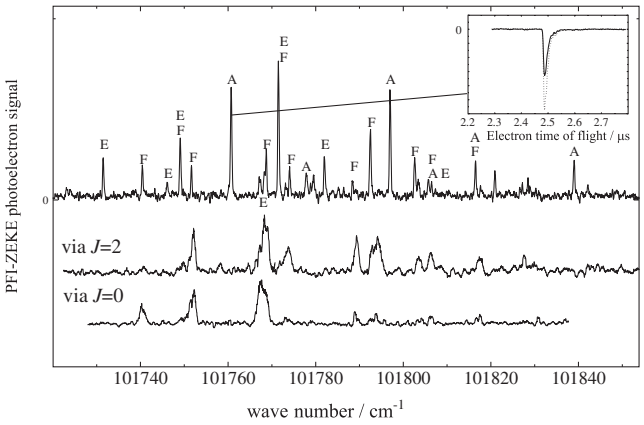

FIG. 2. Top trace: Single-photon PFI-ZEKE PE spectrum of methane in the region of the adiabatic ionization threshold. Lower two traces: two-photon IR + VUV PFI-ZEKE PE spectra recorded via the $J = 2$ and $J = 0$ levels of the ν_3 fundamental. Inset: PFI-ZEKE photoelectron time-of-flight signal recorded with the IR laser resonant with the R(0) transition (full line) or nonresonant with any transition (dotted line). The letters A, E, and F correspond to the experimentally assigned nuclear spin symmetries (A_1, E or F_2).

Two schemes were used to assign the nuclear spin species and the rovibronic symmetry of the ionic levels experimentally. First, the VUV frequency was held at the position of a given line in the single-photon PFI-ZEKE photoelectron spectrum, and the depletion of the photoelectron signal was monitored at the three IR frequencies corresponding to the R(0), R(1), and R(2) lines in the ν_3 fundamental band. A depletion of up to $\approx$ 50% of the original signal indicated that the IR and the VUV photoelectronic transitions had a common lower level. Second, the IR frequency was held at the position of either the R(0), P(1), R(1), P(2), or the R(2) lines of the IR spectrum, and the VUV frequency was scanned across the ionization thresholds. With these two methods, nuclear spin symmetries could be assigned to most lines in the PFI-ZEKE photoelectron spectrum.

The top trace in Fig. 2 gives an overview of the single-photon PFI-ZEKE photoelectron spectrum of CH_4 with the assignment of the nuclear spin symmetry indicated above each line (A for $\Gamma_{rve} = A_1, A_2$, E for $\Gamma_{rve} = E$, F for $\Gamma_{rve} = F_1$, F_2). The next two traces represent the PFI-ZEKE photoelectron spectrum recorded via the $J = 0$ ($\Gamma_{rve} = F_2$) and $J = 2$ ($\Gamma_{rve} = F_2$) intermediate levels. The inset illustrates a typical depletion measurement and compares the electron time-of-flight signal observed when the IR laser frequency is tuned to the position of the R(0) line (full line) or detuned from resonance (dotted line). The reduction of signal by a factor of $\approx$2 in the former case indicates saturation of the IR transition. Similar depletion measurements were carried out to assign the nuclear spin

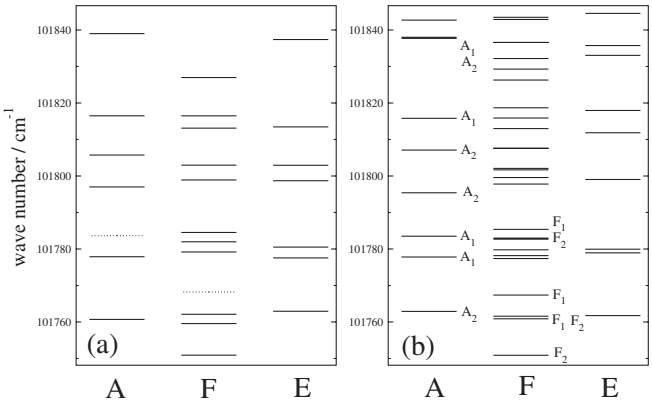

FIG. 3. Comparison of the experimentally determined level structure of CH_4^+ [panel (a)] to the predictions made using the tunneling-rotation Hamiltonian as explained in the text [panel (b)]. Levels at the limit of detection are indicated by dotted lines and the wave number scale is defined relative to the ground state of CH_4.

symmetries of the other lines in the spectrum. From these measurements, the energy level diagram displayed in Fig. 3(a) was derived. The ground state of CH_4^+ is determined to be of F_2 nuclear spin symmetry and the adiabatic ionization energy of CH_4 amounts to 101753.0(15) cm^{-1}.

To treat the tunneling motion between the six C_{2v} minima, a matrix representation is used in the basis of six local functions ϕ_n

$$\phi_n = |n\rangle\chi_n, \qquad n = 1-6 \tag{1}$$

where $|n\rangle$ and χ_n represent the adiabatic electronic function and the ground state vibrational function (a product of 9 harmonic oscillator functions) of the molecule in the nth potential well, respectively. $|n\rangle$ is obtained by diagonalizing the potential term $\mathbf{U}(Q)$ in the Hamiltonian [25]

$$\hat{H}_{\mathrm{JT}} = \sum_{\Gamma\gamma} -\frac{\hbar^2}{2\mu_\Gamma}\frac{\partial^2}{\partial Q_{\Gamma\gamma}^2}\mathbf{C}_\alpha + \mathbf{U}(Q) \tag{2}$$

with

$$\mathbf{U}(Q) = \sum_{\Gamma\gamma}\left(\frac{1}{2}G_\Gamma Q_{\Gamma\gamma}^2\mathbf{C}_\alpha + F_\Gamma Q_{\Gamma\gamma}\mathbf{C}_{\Gamma\gamma}\right), \quad \gamma\in\Gamma, \quad \Gamma = e, t_2 \tag{3}$$

in the diabatic basis $|\xi\rangle, |\eta\rangle, |\zeta\rangle$ of the F_2 electronic state at the six minima of C_{2v} geometry. $Q_{\Gamma\gamma}$, μ_Γ, G_Γ, F_Γ, $\mathbf{C}_\alpha$, and $\mathbf{C}_{\Gamma\gamma}$ are the normal vibrational mode (γ component of the Γ representation), its reduced mass, the sum of the harmonic force constant and quadratic coupling constant for mode Γ, the linear coupling constant, the unit matrix, and the Clebsch-Gordan matrix of the $\Gamma\gamma$ component in the electronic F_2 basis, respectively [25]. The adiabatic electronic functions for the six C_{2v} minima are $\frac{1}{\sqrt{2}}(|\xi\rangle + |\eta\rangle)$, $\frac{1}{\sqrt{2}}(|\xi\rangle + |\zeta\rangle)$, $\frac{1}{\sqrt{2}}(-|\xi\rangle + |\eta\rangle)$, $\frac{1}{\sqrt{2}}(-|\xi\rangle + |\zeta\rangle)$, $\frac{1}{\sqrt{2}}(|\eta\rangle - |\zeta\rangle)$ and $\frac{1}{\sqrt{2}}(|\eta\rangle + |\zeta\rangle)$ and correctly incorporate the effect of the geometric phase.

The tunneling eigenvalues and eigenvectors are the solutions of the determinantal equation

$$\begin{vmatrix}
H_{11}-E & H_{12}-S_{12}E & 0 & -(H_{12}-S_{12}E) & H_{12}-S_{12}E & H_{12}-S_{12}E \\
H_{12}-S_{12}E & H_{11}-E & -(H_{12}-S_{12}E) & 0 & -(H_{12}-S_{12}E) & H_{12}-S_{12}E \\
0 & -(H_{12}-S_{12}E) & H_{11}-E & H_{12}-S_{12}E & H_{12}-S_{12}E & H_{12}-S_{12}E \\
-(H_{12}-S_{12}E) & 0 & H_{12}-S_{12}E & H_{11}-E & -(H_{12}-S_{12}E) & H_{12}-S_{12}E \\
H_{12}-S_{12}E & -(H_{12}-S_{12}E) & H_{12}-S_{12}E & -(H_{12}-S_{12}E) & H_{11}-E & 0 \\
H_{12}-S_{12}E & H_{12}-S_{12}E & H_{12}-S_{12}E & H_{12}-S_{12}E & 0 & H_{11}-E
\end{vmatrix} = 0, \tag{4}$$

where $H_{11} = \langle\chi_1|\hat{H}|\chi_1\rangle$, $H_{12} = \frac{1}{2}\langle\chi_1|\hat{H}|\chi_2\rangle$, and $S_{12} = \frac{1}{2}\langle\chi_1|\chi_2\rangle$. The permutation symmetry requires that $H_{ii} = H_{11}$ for all i and $H_{ij} = H_{12}$ for $i \neq j$. $\langle n|m\rangle$ is either 1, 1/2, $-1/2$, or 0, as can be derived from the six adiabatic electronic wave functions listed above. The solutions of the determinantal equation are two sets of triply degenerate levels (F_2 and F_1):

$$E_{F_2} = \frac{H_{11}+2H_{12}}{1+2S_{12}} \quad \text{and} \quad E_{F_1} = \frac{H_{11}-2H_{12}}{1-2S_{12}} \tag{5}$$

separated by a tunneling splitting denoted δ below. A treatment of the tunneling problem without consideration of the composition of the electronic functions gives a determinantal equation similar to Eq. (4) but in which all nonvanishing off-diagonal elements are $H_{12} - S_{12}E$. In this case, tunneling splits the ground state into three levels with energies

$$E_{A_1} = \frac{H_{11}+4H_{12}}{1+4S_{12}}, \quad E_{F_2} = H_{11}, \quad E_E = \frac{H_{11}-2H_{12}}{1-2S_{12}}. \tag{6}$$

The geometric phase thus has a profound effect on the energy level structure.

To treat the rotational structure in the lowest tunneling pair, it is convenient to set up the rotational Hamiltonian in a global axis system used for all six minimum structures in analogy to the treatment of the rotational motion of molecules in local mode representation [22]. For each C_{2v} structure, the rotational Hamiltonian is obtained by suitable rotation of the global system so that it coincides with the corresponding principal axis systems of the different minima as indicated in Fig. 1 for the equilibrium structure 1. One obtains for this structure

$$\frac{\hat{H}_{(1)}^{\mathrm{rot}}}{hc} = \frac{1}{2}(B+C)(\hat{J}_x^2+\hat{J}_y^2) + \frac{1}{2}(B-C)(\hat{J}_x\hat{J}_y + \hat{J}_y\hat{J}_x) + A\hat{J}_z^2. \tag{7}$$

The rotational Hamiltonian for the other structures can be obtained similarly.

The effective tunneling-rotation Hamiltonian in the basis of the eigenstates of Eq. (4) is

$$\hat{H}_{\mathrm{rve}} = U^T\hat{H}^{\mathrm{rot}}U + \hat{H}_{\mathrm{ve}}, \tag{8}$$

where $\hat{H}^{\mathrm{rot}}$ is a diagonal matrix of rotational operators of the form of Eq. (7) for the six C_{2v} local structures, and U is the eigenvector matrix of the determinantal Eq. (4). $\hat{H}_{\mathrm{ve}}$ is diagonal with eigenvalues 0 for the F_2 levels and δ for the F_1 levels (see Eq. (5)). The calculated and experimental tunneling-rotation eigenvalues up to $N^+ = 4$ (where N^+ labels the rotational angular momentum of CH_4^+) are compared in Fig. 3.

The values of the constants A, B, C, IE/hc, and δ (6.4(5), 5.5(4), 4.0(5), 101753.0(15), and 16.4(40) cm^{-1}) were obtained from a least-squares fit to the six lowest

levels of A symmetry and the four lowest levels of E symmetry. There is a one-to-one correspondence between the calculated and experimental values of the levels of A and E symmetry up to $N^+ = 3$. The calculations predict more F levels than observed experimentally, but the grouping of calculated F levels closely reflects the experimental structure, and it is likely that not all levels could be observed as a result of the resolution and sensitivity limits of the experiment. In particular, the upper tunneling component of the $N^+ = 0$ state around 101768 cm^{-1} could not be unambiguously detected at our experimental sensitivity.

The effective tunneling-rotation Hamiltonian outlined above can be expected to accurately describe the rovibronic structure of the lowest two vibronic states if the barriers separating the equivalent minima are high. In this case, the vibronic wave functions are strongly localized in the minima, and the tunneling splitting becomes negligible. The predicted level structure indeed converges to that of a simple asymmetric top in which each level is sixfold degenerate. In the case of a large tunneling splitting, one obtains two distinct triply degenerate vibronic states with their own rotational structure. In the intermediate situation, when the tunneling splitting becomes comparable to the rotational intervals, additional couplings occur between the rotational, the pseudorotational, and the electronic angular momenta which are not included in the effective Hamiltonian used here. The present Hamiltonian only includes rovibronic coupling terms of the form $\hat{J}_\alpha \hat{J}_\beta$ with E and F_2 symmetry within each of the tunneling states and E and F_2 terms connecting them. Additional terms that are allowed by symmetry, but are not contained in our effective Hamiltonian, are all those of symmetry F_1 that are proportional to $\hat{J}_\alpha$ and represent Coriolis interactions. In the present case, the time scale for tunneling is of the same order of magnitude as the period of molecular rotation. Therefore, the effect of couplings between the pseudorotation and the end-over-end rotation is expected to be significant, and the effective Hamiltonian is not flexible enough for an exact agreement with the experimental data to be obtained. An alternative to the present approach would consist of including all rovibronic coupling terms allowed by symmetry and adjusting their coefficients [26].

Considering the approximate nature of the theoretical treatment, the agreement between calculated and experimental level positions is sufficient for the following conclusions to be drawn: (1) The lowest observed rovibronic level of CH_4^+ is an F_2 level, in agreement with the tunneling calculations including the geometric phase. (2) A triply degenerate ground rovibronic state is also compatible with the expectation that the vibronic ground state should have the same symmetry as the degenerate electronic state. (3) The ground state of CH_4^+ is a tunneling doublet of two triply degenerate levels split by 16.4(40) cm^{-1}. (4) The value of the tunneling splitting is larger than the value inferred from one-dimensional pseudorotational calculations [16] but is compatible with estimates of proton exchange rates from ESR measurements [11]. These results imply that the tunneling motion in the ground state of CH_4^+ actually connects six equivalent minima and constitute the first experimental proof for the C_{2v} geometry of CH_4^+.

We thank Professor M. S. Child (Oxford) and Professor J. T. Hougen (NIST, Gaithersburg) for useful discussions. This work is supported by ETH Zurich and the Swiss National Science Foundation.

[1] I. Bersuker, *The Jahn-Teller Effect* (Cambridge University Press, Cambridge, 2006).
[2] *Conical Intersections*, edited by W. Domcke, D. R. Yarkony, and H. Köppel, Adv. Ser. in Phys. Chem. Vol. 15 (2004).
[3] G. Herzberg and H. C. Longuet-Higgins, Discuss. Faraday Soc. **35**, 77 (1963).
[4] M. Keil *et al.*, J. Chem. Phys. **113**, 7414 (2000).
[5] H. von Busch *et al.*, Phys. Rev. Lett. **81**, 4584 (1998).
[6] D. T. Vituccio, O. Golonzka, and W. E. Ernst, J. Mol. Spectrosc. **184**, 237 (1997).
[7] B. E. Applegate, A. J. Bezant, and T. A. Miller, J. Chem. Phys. **114**, 4869 (2001).
[8] R. Lindner, K. Müller-Dethlefs, E. Wedum, K. Haber, and E. R. Grant, Science **271**, 1698 (1996).
[9] The commonly used label for the JTE still employs the letters T or t to designate triply degenerate electronic states and vibrational modes, respectively, rather than the recommended F and f labels used in the remainder of this article.
[10] L. B. Knight, Jr., J. Steadman, D. Feller, and E. R. Davidson, J. Am. Chem. Soc. **106**, 3700 (1984).
[11] L. B. Knight, Jr. *et al.*, J. Chem. Phys. **103**, 3377 (1995).
[12] J. W. Rabalais, T. Bergmark, L. O. Werme, L. Karlsson, and K. Siegbahn, Phys. Scr. **3**, 13 (1971).
[13] A. W. Potts and W. C. Price, Proc. R. Soc. A **326**, 165 (1972).
[14] R. Signorell and F. Merkt, J. Chem. Phys. **110**, 2309 (1999).
[15] R. Signorell, M. Sommavilla, and F. Merkt, Chem. Phys. Lett. **312**, 139 (1999).
[16] R. Signorell and F. Merkt, Faraday Discuss. **115**, 205 (2000).
[17] R. F. Frey and E. R. Davidson, J. Chem. Phys. **88**, 1775 (1988).
[18] W. Meyer, J. Chem. Phys. **58**, 1017 (1973).
[19] M. N. Paddon-Row, D. J. Fox, J. A. Pople, K. N. Houk, and D. W. Pratt, J. Am. Chem. Soc. **107**, 7696 (1985).
[20] F. Marinelli and M. Roche, Chem. Phys. **146**, 219 (1990).
[21] M. S. Reeves and E. R. Davidson, J. Chem. Phys. **95**, 6551 (1991).
[22] M. S. Child and Q. Zhu, Chem. Phys. Lett. **184**, 41 (1991).
[23] G. Reiser, W. Habenicht, K. Müller-Dethlefs, and E. W. Schlag, Chem. Phys. Lett. **152**, 119 (1988).
[24] A. H. Kung, S. Fei, and H. L. Strauss, Appl. Spectrosc. **50**, 790 (1996).
[25] I. B. Bersuker and V. Z. Polinger, Sov. Phys. JETP **39**, 1023 (1974).
[26] N. Ohashi and J. T. Hougen, J. Mol. Spectrosc. **121**, 474 (1987).